Mechanism of Water Vapor Transport through PET/AlO_xN_y Gas Barrier Films

Ahmet G. Erlat, Bernard M. Henry,* Chris R. M. Grovenor, and Andrew G. D. Briggs

Department of Materials, University of Oxford, Parks Road, Oxford OX1 3PH, U.K.

Richard J. Chater

Department of Materials, Imperial College, London SW7 2BP, U.K.

Yusuke Tsukahara

Technical Research Institute, Toppan Printing Co., Ltd., Sugito-machi, Kitakatsushika-gun, Saitama 345, Japan

Received: July 31, 2003; In Final Form: November 11, 2003

Thin, transparent aluminum oxide coatings on polymers are used widely to improve the gas barrier properties of commodity polymers in the food packaging, pharmaceutical, and organic display technologies. Recently we introduced reactively sputtered aluminum oxynitride coatings on poly (ethylene terephthalate) as a novel alternative to oxide coatings and have shown that they possess, in particular, superior water vapor permeation resistance. In this paper we give a detailed account of how altering the oxynitride morphology and chemistry by varying the magnetron sputtering conditions can directly alter the water vapor barrier performance but has little effect on oxygen permeation. Analysis of these films has also been extended to comparisons with titanium oxynitride and aluminum oxide layers on polymer substrates. In addition to gas permeation measurements and activation energy calculations, a variety of techniques such as atomic force microscopy, scanning electron microscopy, X-ray photoelectron spectroscopy, Rutherford backscattering, and secondary ion mass spectroscopy have been used to correlate the barrier performance to the morphology and chemistry of the films in a more complete model for water vapor permeation.

1. Introduction

The application fields for thin inorganic gas barrier films deposited on polymers cover a wide and diverse area of applications such as food, pharmaceutical, medical, and potentially optoelectronics packaging. Research into this type of composite films is mainly focused on enhancing the oxygen and water vapor barrier performance by optimizing deposition conditions[1] or by modifying the polymer surfaces prior to deposition to minimize potential defect sites.[2] The current requirement for OLEDs demands coatings with exceedingly low oxygen and water vapor transmission rates (OTR and WVTR) of the order of 10^{-3} cc/m^2/day and 10^{-6} g/m^2/day, respectively.[3] To achieve this extremely challenging target, it is crucial to understand the mechanisms by which these species permeate, and especially for water vapor permeation, this understanding is not well developed. For the most widely used barrier coatings, AlO_x and SiO_x, there are indications that the film microstructure and composition have a pronounced effect on the mechanisms by which water vapor permeates. [4−6] Furthermore, exploration of the properties of silicon nitride and oxynitride coatings has shown that inclusion of nitrogen offers a very significant improvement in barrier properties for oxygen[7] and water vapor permeation.[7−9] However, the common method for depositing these latter coatings is plasma enhanced chemical vapor deposition (PECVD) requiring the use of silane as a precursor, which may make this method commercially unattractive for the production of large area barrier films.[7] We have shown recently that similar improvements can be obtained in AlO_xN_y coatings on PET produced by reactive magnetron sputtering.[10,11] Thus there is a growing body of data that suggests that it could be possible to tailor coatings with the desired water vapor barrier performance by compositionally modifying traditional coatings such as AlO_x or SiO_x.

TABLE 1: Five Groups of Coatings Produced by Altering the Sputtering Pressure and Deposition Power[a]

samples	power (W)	P_{total} (Pa)	deposition rate (nm/s)
A	850	0.56	0.25
B	850	0.36	0.38
C	850	0.30	0.45
D	850	0.28	0.43
E	550	0.28	0.34

[a] (A) was produced without any process control (i.e., at a fixed N_2/Ar ratio, the power at 850 W) and those of (B) and (C) were produced by plasma emission monitoring and varying the nitrogen partial pressure at 850 W. (D) and (E) were produced by keeping the total pressure (Ar + N_2) constant and varying the sputtering power from 850 W to 550 W.

In this paper we aim to offer an improved model for the mechanism of water vapor permeation through PET/AlO_xN_y gas barrier films by combining our preliminary results[10,11] with new structural, chemical, and gas permeation data.

2. Experimental Methods

Medium frequency (40 kHz) ac reactive magnetron sputtering, utilizing a coaxial dual magnetron source with commercial Al targets, was used to produce a range of AlO_xN_y coatings on untreated, optical grade commercial poly(ethylene terephthalate) (PET) 50 μm thick, Melinex, and for some experiments on n-type Si(100) wafers. In total, five categories of coatings were produced, as shown in Table 1, by altering the sputtering

10.1021/jp036244y CCC: $27.50
Published on Web 12/20/2003

pressure and deposition power to induce changes in the nanomorphology and chemical composition. The first two categories of coatings are those (A) produced without any process control (i.e., at a fixed N_2/Ar ratio, keeping the power at 850W[10]) and those (B and C) produced by plasma emission monitoring (PEM) and varying the nitrogen partial pressure again at 850 W.[11] In producing samples of category A,[10] it was realized that tailoring AlO_xN_y chemical composition in a controlled manner was not possible due to the unregulated amount of residual oxygen in the chamber ambient (at base pressures around 10^{-3} Pa). Therefore the use of PEM feedback control, normally used to control the reactive sputtering of coatings such as AlO_x in the hysteresis region,[12] proved effective in minimizing the effect of unregulated oxygen and therefore in controlling the nitrogen partial pressures for sample categories B and C. Finally, the other two AlO_xN_y coatings (D and E) were produced by keeping the total pressure ($Ar + N_2$) constant and varying the sputtering power from 850 to 550 W.

Oxygen transmission rate (OTR) measurements on these films were performed using an Oxtran 2/20 permeation instrument (Modern Controls Inc., Minneapolis, MN) at 30 °C and 0% relative humidity (RH). Water vapor transmission rate (WVTR) measurements were taken at 30 °C and 100% RH with a Permatran W 3/31 (Modern Controls, Inc.). Measurements were taken at 10−40 °C for OTR and at 25−45 °C for WVTR to assess the temperature dependence of oxygen and water vapor permeation rates through the gas barrier films. The samples were masked with aluminum foil to define a 5 cm^2 gas exposure area for both types of gas transmission measurements.

The thicknesses and refractive indices of the AlO_xN_y layers on Si were obtained using a Rudolph Auto EL-II Ellipsometer, operated at a wavelength of 632.8 nm and 70° incidence angle. A scanning proton microprobe (SPM) with a 1.6 MeV proton beam was used to study the barrier layer composition. Proton-induced X-ray emission (PIXE) provided identification of the elements present, and Rutherford Backscattering (RBS) analysis enabled quantitative elemental analysis.

The surface morphology of the barrier coatings was examined using atomic force microscopy (AFM). A Model CP, Park Scientific Instruments (Sunnyvale, CA) AFM operated in contact mode provided topographical images of the AlO_xN_y coatings as well as surface roughness measurements. Si tips with a radius of ~10 nm were used for this analysis.

Water wettability of the coatings and the PET substrate, before and after exposure to a nitrogen plasma, were performed by utilizing the sessile drop method[10] to obtain contact angle data. Drops were formed on an area of 8 mm in diameter at an ambient of 22 °C.

An investigation of the chemical interaction between the permeating water molecules and AlO_xN_y films was performed using secondary ion mass spectrometry (SIMS). Sputtered AlO_xN_y films of average coating thickness 43 nm were placed in a Mocon Permatran W3/31 and exposed to water vapor containing 10 at. % ^{18}O, D_2O, and normal water. The films remained in the test cells for over 50 h and the monitoring of the transmission values confirmed that a considerable flux of water vapor had permeated through the composites. SIMS analysis was used to investigate the elemental distribution in the barrier coating. Depth profiles were obtained on an Atomika 6500 instrument, using a 3 keV Xe^+ primary ion beam directed at normal incidence to the AlO_xN_y surface. Primary ion currents of 10 nA were rastered into an area 250 μm^2 and the insulating sample was flooded by an electron beam from a gun operating at 1 keV with a beam current of 1 mA. The profile data were taken from the central 30% of the crater area to avoid contributions from the crater walls.

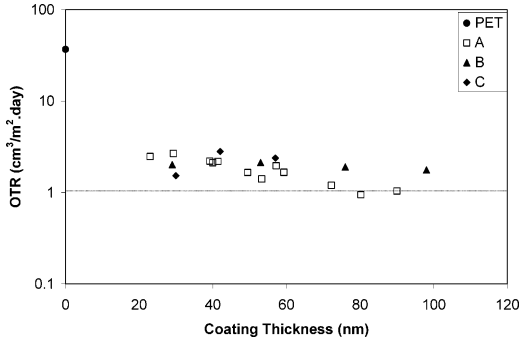

Figure 1. Oxygen transmission rate (OTR) values for PET/AlO_xN_y films in sets A, B, and C as a function of coating thickness and in comparison to the OTR value for bare PET substrate.

For an investigation of the effect of micron-scale defects on barrier properties, 100 μm thick PET substrates obtained from Toray Co., Ltd, were used.

3. Results and Discussion

As is clear from Table 1, changing the deposition conditions can produce AlO_xN_y coatings at significantly differing deposition rates, with the expected trend toward higher values as the total pressure decreases and the deposition power increases.[13] Here we are primarily interested in the effect of this trend on the morphology and chemical composition of the produced AlO_xN_y coatings and the influence of these changes on gas permeation properties.

3.1. Oxygen Permeation. Oxygen transmission rate (OTR) values for PET/ AlO_xN_y films of sample sets A, B, and C are plotted as a function of coating thickness in Figure 1. It is clear from this figure that films in all three sets show a similar oxygen permeation performance despite the variations in deposition conditions (Table 1). In previous publications[10,11] we have identified the main pathways for oxygen transmission through these films as (i) micron-scale pinholes of average diameter 1 μm and (ii) sparsely distributed larger defects. We believe that these 2 types of defects are generated by (i) microarcing during deposition and (ii) intrinsic irregularities or damage on the PET surface. In addition, the activation energies calculated for oxygen permeation through films from sets B and C lie in the range 30 ± 2 kJ/mol, which is identical within experimental error to that of uncoated PET (~29 kJ/mol). Our main conclusion from these observations is that all the AlO_xN_y coatings listed in Table 1 contain a significant number of micron-scale defects that provide unhindered permeation pathways for oxygen molecules. Therefore the variations in sputtering parameters, which could create differences in the nanoscale growth and chemical composition of the coatings, do not alter the permeation properties of oxygen which does not interact chemically with the AlO_xN_y.

3.2. Water Vapor Transport. As will be shown in the remainder of this paper, the mechanism of water vapor permeation through AlO_xN_y coatings is more complicated than that of oxygen. Figure 2 shows WVTR vs coating thickness data for sample sets A−C. In contrast to Figure 1, the WVTR values for these sets vary quite substantially, especially for coatings around 30 and 50−60 nm in thickness. It is surprising when series A and B films are compared that the films of set A deposited at a lower rate under higher total pressure show better moisture permeation resistance. The more usual trend is seen in series C, a superior water vapor barrier performance in the films we expect to be denser. We have also measured in series

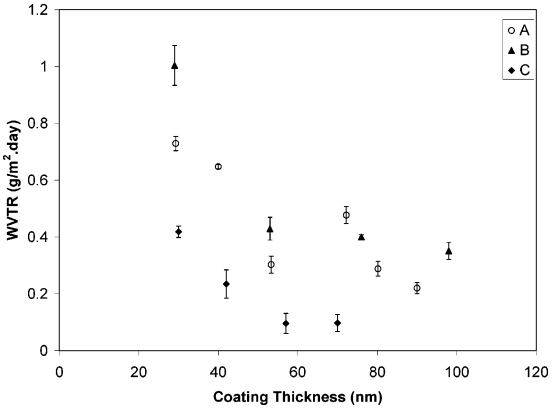

Figure 2. Water vapor transmission rate (WVTR) values for PET/AlO_xN_y films in sets A, B, and C as a function of coating thickness. The WVTR value for PET is 3.89 g m^{-2} day^{-1}, measured at 30°, 100% RH.

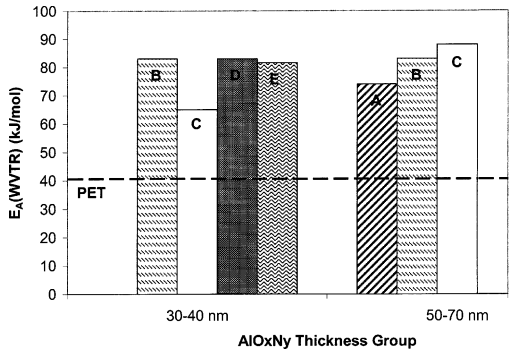

Figure 3. Plot showing a comparison of E_A(WVTR) values for PET/AlO_xN_y films from all sets in Table 1 compared to the value for the bare PET substrate.

D and E the expected increase in WVTR from 0.6 to 1.6 g m^{-2} day^{-1} for 30 nm AlO_xN_y coatings when the sputtering power decreases. This trend supports the general observation from Figure 2 that films deposited at a higher rate possess better water vapor resistance. This effect could be due to the fairly well documented effect that a decrease in total or reactive gas partial pressure and/or increasing the sputtering power in reactive magnetron deposition of thin metal nitride or oxide films leads to formation of denser coatings. Increased deposition rates also result in metal-rich coating compositions.[13]

The calculated activation energy values for water vapor permeation, E_A(WVTR) from WVTR measurements between 25 and 45 °C, for films in two thickness ranges are shown in Figure 3 for all the sample series in Table 1. We have previously suggested[10,11] that the observation that these E_A(WVTR) values for AlO_xN_y barriers are reproducibly considerably higher than those measured for bare PET (40.2 kJ/mol) is due to a chemical interaction of water vapor with the oxynitride material. This conclusion is now reinforced by the new data on series D and E films which also show E_A(WVTR) values higher than 80 kJ/mol. The only significant trend within the thickness groups is that for series C the E_A(WVTR) value increases with increasing thickness.

From the data presented so far, we may conclude that water vapor permeation through our PET/AlO_xN_y films appears to be affected predominantly by interaction with the intrinsic morphology and possibly the composition of the coatings and only to a lesser extent by the micron-scale defects that dominate the permeation of oxygen. To gain a clearer picture of the mechanism of water vapor permeation, we now explore in more detail the effects of micron-scale defects, nanoscale morphology, chemical composition, and possible AlO_xN_y−water vapor interactions on the permeation properties.

3.2.1. Role of Micron-Scale Defects. It is well documented that depositing an acrylate smoothing layer on the polymer substrate prior to the deposition of an inorganic barrier layer helps to reduce the number of micron-scale defects and consequently improves very significantly the oxygen barrier properties.[2] However, the effect these smoothing layers have on the water vapor transmission rates through PET/barrier structures is surprisingly modest. We have explored this effect in more detail to establish the influence of micron-scale defects on the permeation mechanism of water vapor.

For this purpose, 100 μm thick PET substrates, some coated with 1 μm D-acrylate layers (the reaction product of Pentaerythritol triacrylate and hexamethylene diisocyanate)[14] were used. AlO_xN_y films were deposited at a N_2/Ar flow rate ratio of 2:1 at a total pressure of 0.43 Pa and a magnetron plasma power level of 850 W power on both substrates. TiO_xN_y films produced utilizing PEM control at the same pressure and power levels were also deposited on the same substrates. It should be noted that the WVTR values for bare PET and acrylate coated PET/D samples were identical at around 6.7 g m^{-2} day^{-1} and have similar activation energy values of 46 kJ/mol for water vapor permeation.[14] The addition of the smoothing layer by itself thus has no effect on the permeation kinetics. Parts a and b of Figure 4 show the change in WVTR and E_A(WVTR) values when AlO_xN_y, AlO_x, and TiO_xN_y barrier films are grown on PET/D-coat substrates (the AlO_x data are taken from Miyamoto et al.[14]).

For both oxynitride coatings, we can see a substantial decrease in WVTR values as a result of the application of the smoothing layer, accompanied by a significant increase in E_A(WVTR). The former effect suggests that some micron-scale defects have been eliminated as expected,[2] but more intriguing is the increase in activation energy. Combining these two observations, we can conclude that despite the high activation energies for permeation through PET/AlO_xN_y and PET/TiO_xN_y samples compared to those for bare PET that a significant fraction of the total water vapor flux is flowing essentially unhindered (without obstruction by any form of barrier) through micron-scale defects. The elimination of some of these defects by addition of the smoothing layer forces more water molecules to permeate through and interact with the oxynitride coating. In addition, when the data for TiO_xN_y and AlO_xN_y are compared, these effects appear coupled in that the larger percentage decrease in WVTR for TiO_xN_y when the acrylate layer is included is accompanied by a larger increase in the activation energy. Finally, these two figures highlight the differences in the water vapor permeation mechanism through oxynitride and oxide coatings. For AlO_x, despite a 50% decrease in WVTR for layers deposited on PET/D compared to PET/AlO_x samples, there is no significant change in the activation energy for permeation. This observation focuses our attention on the possibility introduced in previous publications[10,11] that N-containing species may be the main sites for interaction of water molecules with the oxynitride coating.

3.2.2. Influence of Fine-Scale Morphology. The results presented in the previous section suggest that a substantial fraction of the water vapor permeates unhindered through micron-scale defects. However, from Figures 2 and 3 it is evident that changing the sputtering conditions also changes the water vapor barrier properties of AlO_xN_y. One reason for this, we believe, is the modification of the fine-scale morphology of the coatings. We have carried out high-resolution AFM studies to identify possible morphological differences between the

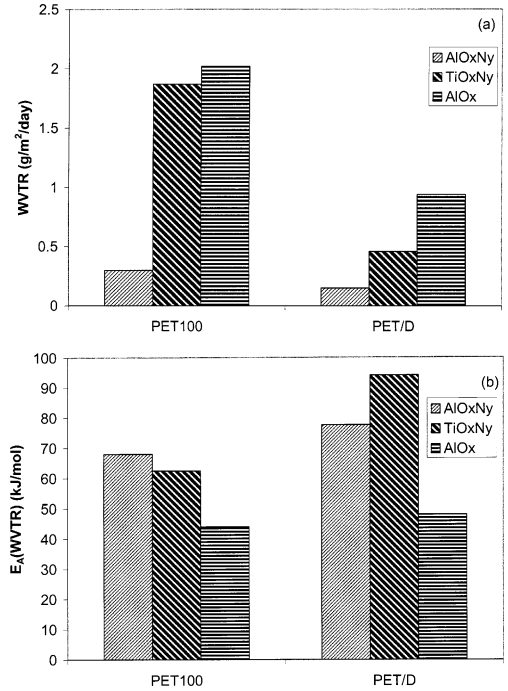

Figure 4. Comparison of (a) WVTR and (b) E_A(WVTR) values for AlO_xN_y, TiO_xN_y, and AlO_x gas barrier coatings deposited on PET (100 μm thick) and PET/D substrates.

coatings in Table 1. Representative 1 μm^2 AFM images are shown in Figure 5a,b for series B and C films to explore the effect of decreasing total sputtering pressure and series E and D for the effect of increasing the sputtering power. For all these images the general morphology is one that would be expected from reactively sputtered coatings on PET at low substrate temperatures (which we try to keep below the 80 °C glass transition temperature of PET), consisting of roughly spherical features (which we will call "grains" hereafter, as is normal in the literature, although there is no crystallographic justification for this title). For the samples deposited at higher deposition rates (C and D) these grains are smaller and much more densely packed, and we note that lower WVTR values are measured for these more densely packed coatings.

Further analysis of these images can also give us an idea of the nucleation and growth processes occurring during deposition, and hence the resulting tortuosity of nanometer-scale permeation pathways through the films thickness. A combination of data from initial growth studies of very thin sputtered AlO_x on PET conducted by Henry et al. using AFM[15] and XPS studies by Cueff et al.[13] show that the coating initially nucleates on preferred sites (with the formation of Al−O−C bonds) and that these nuclei increase in size to form grains of diameter 10−20 nm depending on the sputtering conditions. The growth then proceeds by new grains forming on and between those initial nuclei. What we see in our AFM images are the 3-D representations of the top of the film showing the dome-shaped surfaces of these grains. A very significant feature in these images are the circled areas of dark contrast in Figure 5a which we believe may be the surface appearance of tortuous nanopathways that run throughout the thickness of the coating. From Figure 5a,b we can see that in a densely packed coating these features are comparatively scarce, and any tortuous pathways extending through these films would be expected to have smaller diameters compared to those created in the more loosely packed films. Pathways extending all the way to the PET surface would be significant permeation paths for water vapour and may play a role in chemical interactions of water molecules with the coating as will be discussed in more detail below.

3.2.3. Chemical Factors. To explore the possibility that N-rich sites may be the dominant reaction sites for water molecules, we treated an AlO_x coating on PET with Rf-N_2 plasma at 100 W forward power and 0.27 Pa chamber pressure for periods up

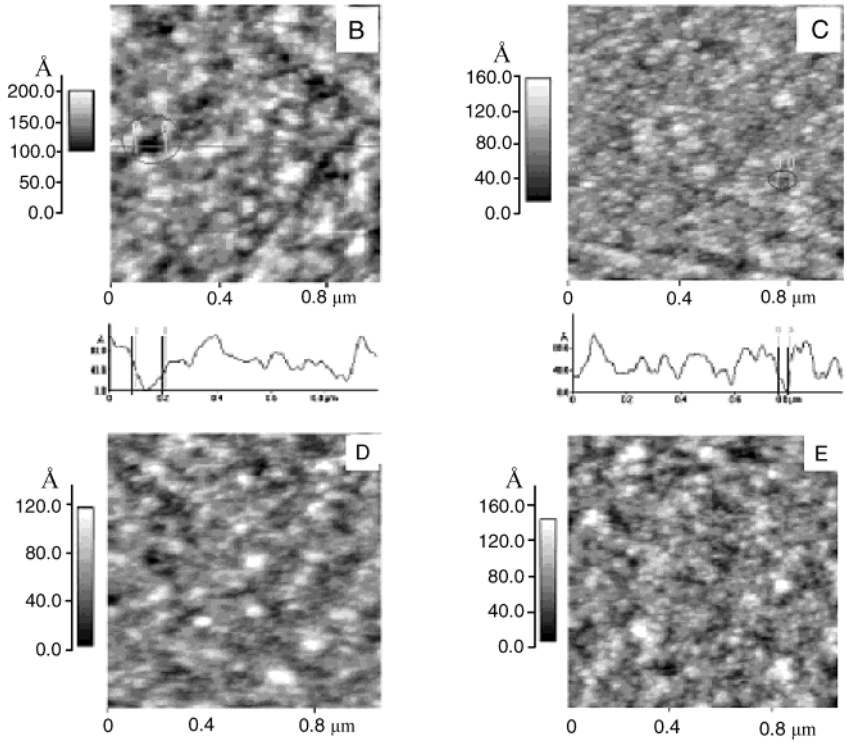

Figure 5. 1 μm^2 AFM images of (a) 53 nm thick AlO_xN_y surface from set B and 42 nm thick AlO_xN_y surface from set C and (b) AlO_xN_y surfaces from sets D and E (both coatings are 30 nm thick). The line scans in (a) show examples of the dark contrast areas believed to be the start of tortuous permeation pathways in the film structures.

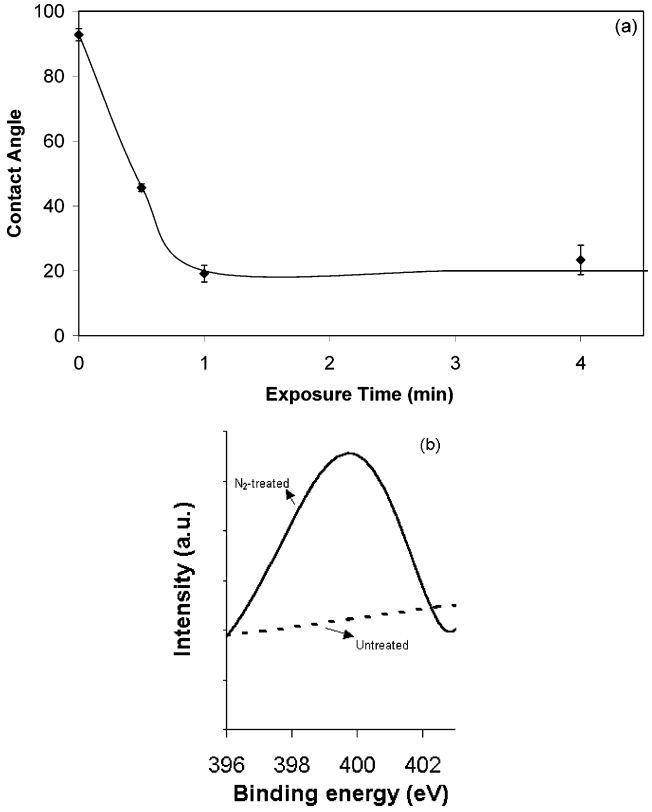

Figure 6. (a) Increased hydrophillicity of the AlO_x surface as a function of exposure time to N_2 plasma. (b) Consequent incorporation of nitrogen shown by the XPS N1s peak after a 4 min exposure. Note that the untreated surface displayed no N-peak.

to 4 min. The N_2 plasma has an average ion energy arriving on the sample surface of 41 eV. The AlO_x surface clearly became more hydrophilic as a result, as is shown in the contact angle vs exposure time plot in Figure 6a. We have also shown by XPS analysis that N species are indeed incorporated on the AlO_x surface as a result of a 4 min plasma treatment, Figure 6b. We might interpret these two pieces of data as offering strong evidence for a chemical interaction of water molecules with N-containing sites on the AlO_x surface.

However, we have to be careful in this interpretation as we have to question how possible plasma *cleaning* of the surface may be influencing the results. A clean oxide surface would be expected to have higher surface energy than a contaminated one and thus a hydrophilic character.[16] Therefore, to clarify if the contact angle of around 20° after 4 min plasma exposure is due to N incorporation, and also to compare surface properties of sputtered AlO_x, AlO_xN_y, and Al, we have performed contact angle measurements on these films immediately after deposition and then after an extended period of time in laboratory ambient. The results are displayed in Figure 7. First we can confirm that the initial hydrophobic nature of untreated AlO_x is due to contamination from the ambient, which takes a considerable period to develop on a newly deposited film, in agreement with Takeda et al.[16] Second, we see that after 1 day in ambient the contact angle on AlO_x rises to around 43°, which is very close to the value after a 30 s N_2 plasma treatment (Figure 6a). We conclude that this length of plasma treatment is only sufficient to clean away some of the surface contamination and can presume that no N is yet incorporated in the surface. However, for treatment times longer than 1 min, the contact angle of around 20° is lower than 30° measured on an uncontaminated AlO_x surface, supporting the conclusion that nitrogen incorporation is now the main factor influencing the wettability of the surface, although we accept that there could also be considerable disruption of surface bonds and relocation of surface atoms that we cannot analyze as well as the N incorporation. From Figure 7 it can also be seen that immediately after deposition the AlO_xN_y surface is more hydrophilic than AlO_x, which also encourages us to consider the role of N in the surface to be important.

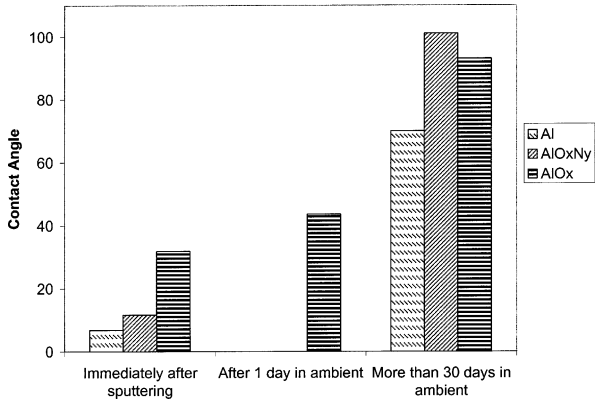

Figure 7. Water contact angle analysis of Al, AlO_xN_y, and AlO_x coating surfaces immediately after growth, after 1 day storage in ambient and after storage in ambient for more than 30 days.

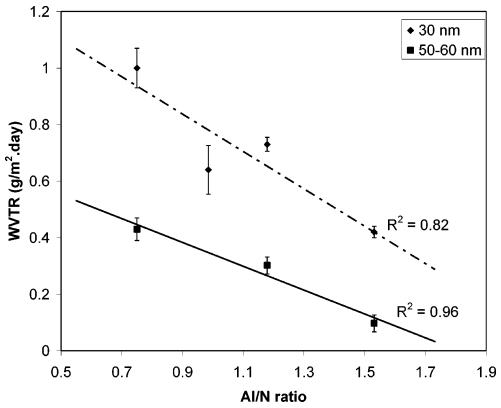

Figure 8. General correlation of WVTR values with Al/N ratio for PET/AlO_xN_y gas barrier films plotted for two AlO_xN_y coating thickness groups, 30 and 50−60 nm. WVTR values are compiled from samples of all sets in Table 1.

We now need to consider the significance of these reaction sites and how they affect the water vapor permeation mechanism. We combine the overall effect of coating composition and morphology on water vapor transport by separating all the PET/ AlO_xN_y samples in Table 1 into two groups of thickness 30 nm and 50−60 nm, and plotting the relationship between WVTR and Al/N ratio (measured by RBS), Figure 8. As is evident from this figure, there is a plausible linear correlation between the two film properties in that the water vapor barrier quality for our AlO_xN_y films improves as the Al/N ratio increases. Bearing in mind that occasionally high E_A(WVTR) values can be measured on samples that are poor moisture barrier coatings, we believe that the following inference can be made from Figure 8. Though some minimum nitrogen content is necessary to attain high E_A values, the N-rich sites acting as energy wells to trap water molecules and hinder their permeation, too high a N-content degrades the permeation properties. In the case of excess nitrogen, especially if the primary transport mechanism is through tortuous permeation paths a few nanometers in diameter, multilayer adsorption of water may be occurring, driven by the high concentration of the trapping

sites. This may lead to surface diffusion along these pore walls or capillary condensation between the walls, which would result in extra water vapor permeation in addition to the molecular flow normally considered to dominate in these materials.[17]

3.2.4. Mechanism of Water Vapor Permeation. Some key points suggested by the experiments described above and some of our main assumptions are as follows:

Micron-scale defects in the coating account for only a small fraction of the total WVTR. If we assume a wholly molecular flux of H_2O (as generally presumed for oxygen) and take a defect radius of 0.5 μm with 700 mm^{-2} density (the data reported for series A in Table 1[10]), and following the defect model of Rossi and Nulman,[18] we calculate that approximately 20% of the measured WVTR flows unhindered through these defects. So we conclude that most of the water vapor flow is not defect-controlled and therefore not predominantly unhindered.

Our coatings contain tortuous pathways a few nanometers in diameter that are of central importance in controlling WVTR values. Denser coatings (narrower and more widely separated pathways) result in lower WVTR values.

The significantly higher activation energies measured for H_2O transmission through the PET/AlO_xN_y films compared to the value for bare PET point to strong chemical interaction of water vapor with the AlO_xN_y coatings. We have shown some evidence that N-rich sites appear to promote these reactions.

The top AlO_xN_y surface (note that the AlO_xN_y surface faces the upstream side in our permeation experiments) if kept in ambient before the permeation test is of a hydrophobic nature. However, this does not necessarily imply that the walls of the tortuous pathways behave similarly. In fact, given the high hydrophillicity of a AlO_xN_y surface uncontaminated by atmospheric contaminants (Figure 7), we will assume that these pore walls have a similar nature and may be the main sites for interactions with water vapor.

The remaining question then is how do these chemical reactions occur and what is their overall contribution to the permeation mechanism? We have studied how the water vapor itself behaves as it permeates through the PET/AlO_xN_y structure. For this purpose three coatings, 43 nm thick, were produced under identical sputtering conditions (similar to those for sample set A) for each to be exposed to water vapor of three different isotopic configurations. All these films had identical refractive index values of 1.87 and SIMS depth profiles for $^{27}Al^-$, $^{16}O^-$, and $^{41}(AlN)^-$ secondary ions showed most importantly a uniform O distribution throughout the 43 ± 2 nm coating thickness after a short initial transient, as can be seen for one of the three samples in Figure 9. The Al^- and AlN^- signals gradually increase throughout the coating thickness.

Of the three coatings, one was exposed to normal water vapor (sample I), one to D_2O (sample II) and the final coating was exposed to water vapor containing 10 at. % ^{18}O (sample III). The samples were oriented so that the AlO_xN_y surface faced the upstream side in the permeation apparatus, and as mentioned in section 2, samples were exposed for over 50 h. A considerable flux of water vapor had permeated through all three samples, as indicated by the measured WVTR value around 0.3 g m^{-2} day^{-1}. The only E_A(WVTR) value measured on these samples was 68 kJ/mol for sample I, which is reasonably consistent with the values in Figure 3. The measurements indicated that these films were good barriers to water vapor permeation, and the high E_A(WVTR) value for sample I suggests that they are

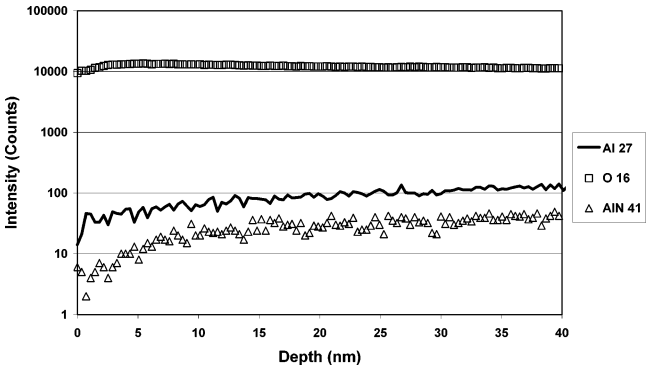

Figure 9. SIMS depth profile showing the distributions for $^{27}Al^-$, $^{16}O^-$, and $^{41}(AlN)^-$ in sample I AlO_xN_y coating.

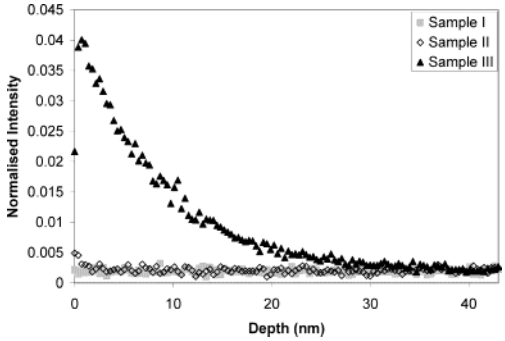

Figure 10. Comparison of normalized mass 18 depth profiles for samples I−III.

suitable for the aim of this experiment: to investigate chemical interactions with the barrier layer.

Figure 10 shows the SIMS depth profile for the mass 18 signal normalized to the ^{16}O signal for samples I−III after exposure to normal, deuterated, and ^{18}O-tagged water vapor, respectively. First, we recall that sample I is the control sample, so the mass 18 profile for this sample is taken as the baseline for the SIMS signal from natural ^{18}O in the oxynitride layer. The natural abundances of ^{16}O and ^{18}O are 99.757 and 0.205%, respectively, giving a $^{18}O/^{16}O$ ratio of 0.002. When the SIMS profiles for samples I and II are compared, it is seen that the two signals are virtually identical. This observation indicates that even if any chemical interaction has occurred between the deuterated water molecules and AlO_xN_y surface, there is no evidence that ^{16}OD species have adsorbed on the coating surface or in the bulk. For sample III which has been exposed to $H_2{}^{18}O$, there is a significantly different profile in which there is a considerable mass 18 accumulation within the AlO_xN_y layer. Because we attribute the source of the mass 18 signal for sample III to the trapping of ^{18}O (originating from $H_2{}^{18}O$), this gives strong evidence for a chemical interaction of water vapor with the AlO_xN_y coating during permeation. When combined with the observation that, when profiling using ions of mass 2, we observed reproducibly that the D species introduced as D_2O are not similarly trapped, this serves as very strong evidence that water vapor dissociates during permeation through the AlO_xN_y coating.

A similar experiment was also conducted for a PET/AlO_x gas barrier film to investigate if any differences could be observed in the water vapor permeation mechanism for AlO_x and AlO_xN_y. The AlO_x sample used is a dc magnetron sputtered, 17 nm thick coating on a 12 μm thick PET substrate.[19] The film has a WVTR value of 0.78 g m^{-2} day^{-1} measured at 30 °C and 100% RH. The calculated E_A(WVTR) value for this film was 58 kJ/mol, a rare PET/AlO_x sample with a significantly

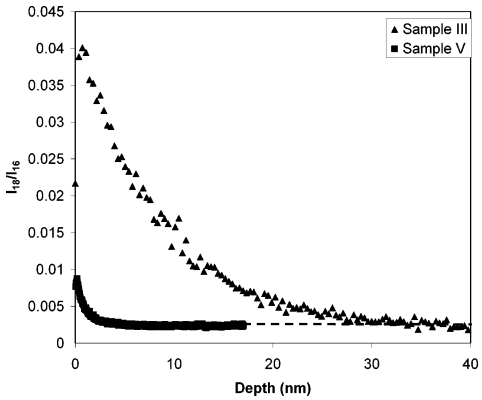

Figure 11. Comparison of normalized mass 18 depth profiles for AlO_xN_y sample III and AlO_x sample V.

higher activation energy for permeation than the value of 42 kJ/mol for bare PET. This time only two identical samples were exposed to normal water and to 10 at. % ^{18}O enhanced water vapor (samples IV and V, respectively). This time the depth profiles were obtained from a PHI adept 1010 SIMS instrument, experimental details for which are given by Henry et al..[19] It should be noted that the mass 18 profile for sample IV is virtually identical to that of sample I, showing no enhancement above the natural background, and will not be reproduced here. Instead, we show in Figure 11 the comparison in normalized mass ion 18 profiles between AlO_xN_y (sample III) and AlO_x (sample V), both exposed to $H_2{}^{18}O$ for the same time. From this figure it can be seen that for the AlO_x sample there does appear to be a modest enhancement of ^{18}O near the surface that may be due to adsorbed ^{18}O as a result of a dissociation reaction. In the only other study of this type, Barocela[20] detected by SIMS analysis of normal and ^{18}O enhanced water vapor-exposed AlO_x films on GaAs an accumulation of ^{18}O in the near surface region ($<6-7$ nm) of a 240 nm thick film. However, he did not attribute this result to any ^{18}O adsorption in the AlO_x and made no comment on the water permeation mechanism. The interesting observation from Figure 11 is that even if there is some evidence of a chemical interaction during water vapor permeation through our PET/AlO_x film, when the depth profile from sample V is compared to that from sample III, it is clear that the *extent* of the interaction observed in the AlO_xN_y sample is much greater both in the normalized ^{18}O concentration and in the depth of the region from which the enhanced signal is detected. This is a strong indication that the water vapor permeation mechanisms for AlO_x and AlO_xN_y are substantially different, and we suggest that this experiment strengthens our contention that the role of nitrogen-rich sites on AlO_xN_y surfaces is to promote chemical interactions with permeating water vapor.

The cumulative effect of this SIMS data leads us to suggest that some water molecules dissociate as they encounter the AlO_xN_y surface, resulting in the entrapment of oxygen species *but not* hydrogen. Studies investigating the role of H/D or $^{16}O/^{18}O$ exchange reactions from dissolved molecular water on oxide surfaces (mostly for silica) prior to diffusion report that these reactions take place only above 500 °C.[21] The idea that H/D exchange may provide a means of diffusion-reaction type flow[21] can be ruled out in our case solely due to the similarities in depth profiles in Figure 10 for samples I and II, exposed to H_2O and D_2O, respectively. The observation of isotopic exchange between oxygen atoms in the permeating water and the oxynitride film would be a definitive sign of dissociation,[22] but given the observations of Doremus[21] on the high-temperature requirement for this type of exchange we do not believe this to

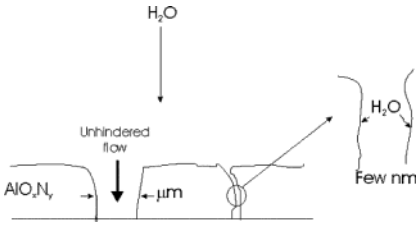

Figure 12. Proposed mechanism of water vapor permeation through PET/AlO_xN_y films.

be a plausible interpretation of the results from our experiments. An alternate process for diffusion of water following dissociation is proton diffusion (proton hopping) through the oxide matrix.[23] Given the findings and assumptions listed at the beginning of this section for the AlO_xN_y coatings, especially the presence of various pathways for permeation and the hydrophobicity of the immediate top surface, this process also seems unlikely. The mechanism therefore we propose is illustrated schematically in Figure 12. We suggest that water molecules arriving on the hydrophobic top surface try to find energetically favorable permeation pathways, the micron-scale defects and smaller tortuous pathways. Once water molecules reach the more influential tortuous pathways, which we know carry about 80% of the flux, they strongly interact with the more hydrophilic pore walls (presumably on N-rich sites), and dissociation of some water molecules occurs, causing local trapping of oxygen. We have shown that there is a considerable flux of water molecules through the PET/AlO_xN_y samples after 50 h exposure, so the noninteracting H-species would then need to re-form into water molecules to complete the permeation process. The mechanism by which this latter phenomena occurs is under investigation, but a possible mechanism, assuming that the very initial dissociation of water is into OH and H adsorbed species, may proceed by the following two reactions:[23]

$$OH(a) + H(a) \rightarrow H_2(g) + O(a) \quad (1)$$

$$2H_2(g) + O_2(g) \rightarrow 2H_2O(g) \quad (2)$$

Equation 1 here both provides a means of explaining the formation of adsorbed (O(a)) oxygen revealed by the ^{18}O SIMS experiment and also represents the activated process of liberating H-species from the pore wall surfaces, and we believe the observed activation energy values are controlled by this reaction. Equation 2 on the other hand may describe the re-formation of water molecules to continue permeation. The permeation environment under 100% RH also contains both N_2 and O_2 gases. The only carrier gas (at 1 atm pressure) on the downstream side of the Permatran apparatus is N_2, so the O_2 concentration is negligible on this side. Therefore, during water vapor permeation there will also be permeation of O_2 through the films, which may provide the necessary oxygen on the backside of the film for eq 2 to proceed.

4. Conclusions

We believe that we have suggested a significantly improved model for the mechanism of water vapor permeation through PET/AlO_xN_y gas barrier films; identifying that water vapor permeates predominantly through the tortuous, nanoscale permeation pathways in the AlO_xN_y structure. The nature of this permeation process we suggest results from the strong chemical interaction of the water molecules with the AlO_xN_y tortuous pore walls possibly at N-rich sites. We further believe that the

reactions are *dissociative* where some oxygen species are trapped and the H_2 permeates essentially unhindered.

This model can be used in two interrelated ways to further improve the barrier properties of polymer/barrier composites toward those required for the application areas described above, especially to achieve the stringent requirements for the encapsulation of optoelectronic devices. One route would be to use the improved understanding of the mechanism in this paper to investigate in more detail the dissociation mechanisms of water vapor during permeation and thereby obtain a better understanding of the atomistic mechanism of water vapor permeation. At the same time, the model can be successfully used to design deposition processes that would produce better barrier materials. The key requirements for this purpose are to increase the density of the coatings as much as possible to reduce the size and number density of tortuous pathways while maintaining an optimum Al/N ratio.

References and Notes

(1) Schiller, S.; Kirchhoff, V.; Schiller, N.; Morgner, H. *Surf. Coat. Technol.* 2000, *125*, 354.

(2) Affinito, J. D.; Gross, M. E.; Coronado, C. A.; Graff, G. L.; Greenwell, E. N.; Martin, P. M. *Thin Solid Films* **1996**, *290*−*291*, 63.

(3) Burrows, P. E.; Graff, G. L.; Gross, M. E.; Martin, P. M.; Shi, M. K., Hall, M.; Mast, E.; Bonham, C.; Bennett, W.; Sullivan, M. B. *Displays* **2001**, *22*, 65.

(4) Deng, C.-S.; Assender, H. E.; Dinelli, F.; Kolosov, O. V.; Briggs, G. A. D.; Miyamoto, T.; Tsukahara, Y. *J. Polym. Sci B: Polym. Phys.* **2000**, *38*, 3151.

(5) Tropsha, Y. G.; Harvey, N. G. *J. Phys. Chem. B* **1997**, *101*, 2259.

(6) Erlat, A. G.; Spontak, R. J.; Clarke, R. P.; Robinson, T. C.; Haaland, P. D., Tropsha, Y., Harvey, N. G.; Vogler, E. A. *J. Phys. Chem. B* **1999**, *103*, 6047.

(7) da Silva Sobrinho, A. S.; Czeremuzskin, G.; Latrèche, M.; Wertheimer, M. R. *J. Vac. Sci. Technol. A* **2000**, *18*, 149.

(8) Vogt, M.; Hauptmann, R. *Surf. Coat. Technol.* **1995**, *74*−*75*, 676.

(9) Lin, H.; Xu, L.; Chen, X.; Wang, X.; Sheng, M.; Stubhan, F.; Merkel, K.-H.; Wilde, J. *Thin Solid Films* **1998**, *333*, 71.

(10) Erlat, A. G.; Henry, B. M.; Ingram, J. J.; Mountain, D. B.; McGuigan, A.; Howson, R. P.; Grovenor, C. R. M.; Briggs, G. A. D.; Tsukahara, Y. *Thin Solid Films* **2001**, *388*, 78.

(11) Erlat, A. G.; Henry, B. M.; Howson, R. P.; Grovenor, C. R. M.; Deng, C.-S.; Briggs, G. A. D.; Tsukahara, Y. *Soc. Vac. Coat. Annu. Technol. Conf. Proc.*, *44th* **2001**, 448.

(12) Kelly, P. J.; Arnell, R. D. *J Vac Sci Technol. A* **2000**, *17*, 945.

(13) Cueff, R.; Baud, G.; Besse, J. P.; Jacquet, M.; Benmalek, M.; Butruille, J. R. *Surf. Coat. Technol.* **1996**, *80*, 96.

(14) Miyamoto, T.; Mizuno, K.; Noguchi, N.; Nijima, T. *Soc. Vac. Coat. Annu. Technol. Conf. Proc.*, *44th* **2001**, 166.

(15) Henry, B. M.; Dinelli, F.; Zhao, K.-Y.; Grovenor, C. R. M.; Kolosov, O. V.; Briggs, G. A. D.; Roberts, A. P.; Kumar, R. S.; Howson, R. P. *Thin Solid Films* **1999**, *355*−*356*, 500.

(16) Takeda, S.; Yamamoto, K.; Hayasaka, Y.; Matsumoto, K. *J. Non-Cryst. Solids* **1999**, *249*, 41.

(17) Cooper, C. A.; Lin, Y. S. *J. Membr. Sci.* **2002**, *195*, 35.

(18) Rossi, G.; Nulman, M. *J. Appl. Phys.* **1993**, *74*, 5471.

(19) Henry, B. M.; Erlat, A. G.; Grovenor, C. R. M.; Deng, C.-S.; Briggs, G. A. D. *Annu. Technol. Conf. Proc.*, *44th* **2001**, 469.

(20) Barocela, E. *J. Vac. Sci. Technol. A* **1986**, *4*, 1893.

(21) Doremus, R. H. *Earth Planetary Sci. Lett.* **1998**, *163*, 43.

(22) Henderson, M. A. *Surf. Sci. Rep.* **2002**, *46*, 1.

(23) J. E. Shelby *Handbook of Gas Diffusion in Solids and Melts*; ASM International: Materials Park, OH, 1996.